Available online at www.sciencedirect.com
ScienceDirect
Journal of Solid State Chemistry 180 (2007) 749–758
JOURNAL OF SOLID STATE CHEMISTRY
www.elsevier.com/locate/jssc

Structural study of VO_x doped aluminium fluoride and aluminium oxide catalysts

Kerstin Scheurell, Gudrun Scholz, Erhard Kemnitz*

Institute of Chemistry, Humboldt University of Berlin, Brook-Taylor-Street 2, Berlin D-12489, Germany

Received 17 August 2006; received in revised form 27 November 2006; accepted 4 December 2006
Available online 8 December 2006

This paper is dedicated to Prof. Dr. Bernhard Luecke on the occasion of his 70th birthday

Abstract

The structural properties of vanadium doped aluminium oxyfluorides and aluminium oxides, prepared by a modified sol–gel synthesis route, were thoroughly investigated. The influence of the preparation technique and the calcination temperature on the coordination of vanadium, aluminium and fluorine was analysed by different spectroscopic methods such as Raman, MAS NMR and ESR spectroscopy. In all samples calcined at low temperatures (350 °C), vanadium coexists in two oxidation states V^{IV} and V^{V}, with V^{IV} as dominating species in the vanadium doped aluminium oxyfluorides. In the fluoride containing solids aluminium as well as vanadium are coordinated by fluorine and oxygen. Thermal annealing of 800 °C leads to an extensive reorganisation of the original matrices and to the oxidation of V^{IV} to V^{V} in both systems.

Keywords: Vanadium doped aluminium oxyfluoride; Vanadium doped aluminium oxide; Sol–gel synthesis; Raman; MAS NMR; ESR

1. Introduction

Vanadium oxide containing solids have been widely investigated as catalysts for selective oxidation reactions [1–9]. The performance of such catalysts strongly depends on the coordination and dispersion of the VO_x species as well as on the surface properties of the solid system [10,11]. Especially the surface acidity is of particular importance for the catalytic behaviour. It has been established that the presence of Brønsted acid sites leads to a lower selectivity towards the desired products of partial oxidation processes, since total oxidation reactions are favoured [12]. Therefore, Lewis acid vanadium catalysts without Brønsted acid sites are required for a more selective activation of organic reactants.

Alumina is a common support for vanadium containing catalysts [2,13,14], but rarely used as host lattice for incorporating VO_x species. If vanadium is successfully introduced into the bulk, a high degree of dispersion of VO_x species can be achieved. Unfortunately, the structural diversity of alumina is huge and on the surface exist Lewis acid as well as Brønsted acid sites. In general, the formation of Brønsted sites can be avoided by employing aluminium fluorides or oxyfluorides instead of alumina as host lattices.

From the preparation of aluminium fluorides in aqueous solutions crystalline phases with small specific surface area (~30 m^2/g) and relatively low Lewis acidity are usually obtained [15]. Therefore, the conventional sol–gel technique has to be modified for preparing high-surface aluminium fluorides as well as VO_x doped aluminium fluorides. In a first step, a gel has to be produced from aluminium alkoxide and a non-aqueous HF solution [16]. The subsequent calcination must be performed under mild conditions in order to obtain fluoride catalysts with high specific surface areas and Lewis acid surfaces [17].

The structural investigation of the less ordered vanadium doped oxides and X-ray amorphous vanadium doped fluorides is rather difficult. In principle, the coordination of aluminium and vanadium can be analysed by FTIR and Raman spectroscopy. Due to the large extent of disorder in

*Corresponding author. Fax: +49 30 2093 7277.
E-mail address: erhard.kemnitz@chemie.hu-berlin.de (E. Kemnitz).

0022-4596/$ - see front matter
doi:10.1016/j.jssc.2006.12.003

the samples, however, the vibration bands of the VO_x species are very broad and difficult to interpret.

More distinct conclusions can be drawn from local structural probe methods such as magic angle spinning (MAS)NMR and ESR spectroscopies. Especially the first method mentioned applies for supplying information on the structural environment of ^{27}Al, ^{19}F, and ^{51}V even in amorphous solids, respectively. Moreover, the oxidation state of the VO_x species can be analysed by a combination of ESR and NMR spectroscopy.

Here, we report on the structural characterisation of vanadium doped aluminium oxides and oxyfluorides prepared by a modified sol–gel technique. Common structural properties and differences between the two systems are investigated by X-ray diffraction, Raman, MAS NMR and ESR spectroscopies. The attention is focused on the comparison of the structural environment of ^{27}Al, ^{51}V, and ^{19}F sites, the distribution of VO_x species in the host lattice and the oxidation state of vanadium. Moreover, the less ordered materials were calcined at 800 °C in order to study the effect of further annealing on the coordination of aluminium, vanadium and fluorine as well as to initiate crystallisation processes.

2. Experimental

2.1. Sample preparation

2.1.1. VO_x doped aluminium oxyfluorides

The synthesis of the vanadium doped high surface aluminium oxyfluorides is described in detail elsewhere [17]. It starts from aluminium triisopropoxide (Aldrich, ⩾98%) dissolved in dried isopropylalcohol and its fluorination with anhydrous HF in diethyl ether. The fluorine to oxygen ratio in the bulk was adjusted by the HF to $Al(OiPr)_3$ ratio. Employing an excess of $Al(OiPr)_3$, incompletely fluorinated aluminium alkoxide fluoride precursor phases can be prepared in which the remaining Al-O*i*Pr-groups may be used as anchor groups for further functionalisation with vanadylalkoxides (Aldrich, ⩾98%). In this way, highly dispersed VO_x species, homogeneously distributed in the formerly originated open frame of $AlF_x(OiPr)_{3-x}$ were formed. The final calcination of the obtained solids was performed in air at 623 K leading to a VO_x doped aluminium fluoride (V/AlF_xO_y) with a fluorine content of 50.3 wt%. Calcination at 800 °C reduced the fluorine content to 10.7 wt%.

2.1.2. VO_x doped aluminium oxides

Aluminium triisopropoxide (Aldrich, ⩾98%) was suspended in water in a molar ratio of $Al(OiPr)_3$:H_2O of 1:110. In order to induce the hydrolysis, the suspension was heated under reflux for 2 h at 363 K. After the formation of an γ-AlOOH precipitate, concentrated nitric acid (molar ratio: $Al(OiPr)_3$:HNO_3 as 1:0.15) was added and the hydrolysis was completed by further heating for 6 h under the conditions above. The addition of nitric acid leads to the formation of a clear γ-AlOOH sol, which can be mixed with the vanadylalkoxide ($VO(OPr)_3$, Aldrich, ⩾98%). After cooling down and overnight aging, the solvent was removed under vacuum (by means of a rotary evaporator). The obtained precursor was calcined for 5 h at 623 K in air flow (20 mL/min) leading to a VO_x doped oxide (V/AlOOH).

The following sample codes are used for the vanandium doped aluminium oxyfluorides and -oxides:

VAlF 20 350 VAlO 20 350

VAlF 20 800 VAlO 20 800

VAlF 20 and VAlO 20 indicate the vanadium doped aluminium oxyfluorides (VAlF) and -oxides (VAlO) with 20 mol% vanadium. The calcination temperatures used are 350 and 800 °C.

The following were studied as reference materials:

HS-AlF_3 (**h**igh **s**urface AlF_3, prepared by the sol–gel route without VO_x doping [16]), VAlO 00 350 (a sample prepared without vanadium), V_2O_5 (Aldrich ⩾99.6%) and VOF_3 (Aldrich, 99%).

2.2. Sample characterisation

2.2.1. XRD

XRD measurements were performed using the FMP 7 equipment (Rich. Seiffert & Co., Freiberg) with Cu$K\alpha$ (Cu$K\alpha_{1,2}$, $\lambda = 1.5418$ Å) radiation. Phases were identified by comparison with the ICSD powder diffraction file [18].

2.2.2. MAS NMR

^{19}F, ^{27}Al and ^{51}V MAS NMR spectra were recorded on a Bruker AVANCE 400 spectrometer ($\nu_{19F} = 376.4$ MHz; $\nu_{27Al} = 104.3$ MHz, $\nu_{51V} = 105.2$ MHz) using both a 2.5 and a 4 mm magic angle spinning (MAS) probe (Bruker Biospin) allowing spinning frequencies up to 35 and 15 kHz, respectively.

^{19}F MAS NMR spectra were recorded with a $\pi/2$ pulse duration of p1 = 1.74 μs, a spectrum width of 400 kHz and a recycle delay of 60 s. The isotropic chemical shifts δ_{iso} of ^{19}F resonances are given below with respect to the $CFCl_3$ standard.

For the $\pi/2$ pulse experiments, existent background signals of ^{19}F could be completely suppressed with the application of a phase-cycled depth pulse sequence according to Cory and Ritchey [19].

^{27}Al MAS NMR ($I = 5/2$) spectra were recorded with an excitation pulse duration of 1 μs, corresponding to π/8 of the reference. A 1 M aqueous solution of $AlCl_3$ was used as reference for the chemical shift of ^{27}Al. The recycle delay was chosen as 1 s and an accumulation number between 256 and 600 was used for an appropriate signal-to-noise ratio.

^{51}V MAS NMR ($I = 7/2$) spectra were recorded with a $\pi/12$ excitation pulse duration of 1.0 μs. $VOCl_3$ was used as reference for the chemical shift of ^{51}V. The recycling delay was chosen as 1 s. The accumulation number was different in dependence on the V^V content of the samples. Numbers between 600 and 4000 were necessary for the oxide samples, whereas accumulations up to 85,000 have been necessary for the fluoride samples using the 4 mm probe.

The solid state NMR spectra were handled using the Bruker XWIN-NMR software. Simulations were performed with the DMFIT-software [20].

2.2.3. ESR

ESR spectra were taken at 298, 77 K and in part at 4.2 K in X-band with an ERS300 spectrometer (Zentrum für Wissenschaftlichen Gerätebau, Berlin-Adlershof, Germany). A small sample of MgO/Cr^{III} mounted inside the cavity served as a reference for the frequencies and amplitudes of the signals. The modulation amplitude of 0.125 mT was applied for all measurements.

2.2.4. Raman spectroscopy

RAMAN spectra were recorded with a DILOR XY instrument using the 514 nm line of an Ar–ion laser (Carl Zeiss Jena). The laser was operated at a power level of 2 mW.

3. Results

3.1. XRD

X-ray diffraction measurements of both, undoped and VO_x doped fluorides give clear evidence of the amorphous character of both samples (not expl. shown here). For the oxide samples, broad reflections are obtained both for the undoped (VAlO 00 350) and VO_x doped solid (Fig. 1). Differences between the two samples are marginal and only to be seen in the low 2θ range. The maxima of the reflections are at the typical positions of AlOOH (boehmite). Usually, such samples are named as pseudoboehmites, i.e. less ordered boehmites, with a water content of 1.3–1.8 mol H_2O/mol Al_2O_3 [21].

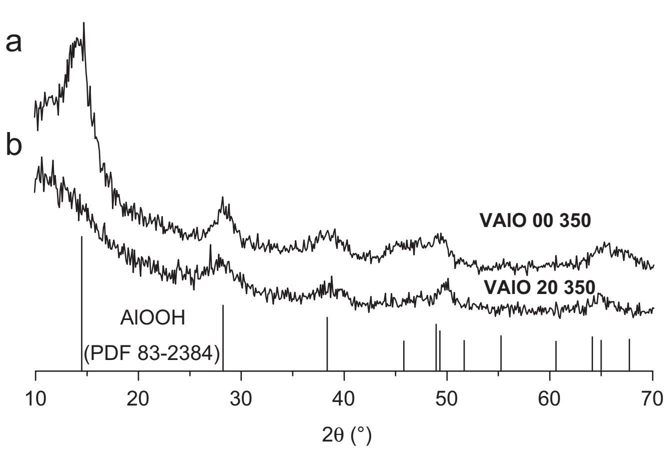

Fig. 1. X-ray diffraction patterns for (a) VAlO 00 350 and (b) VAlO 20 350.

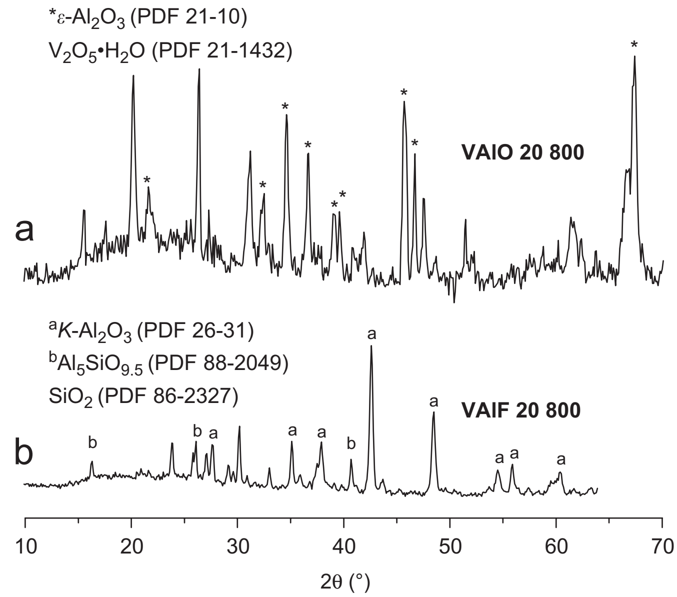

Fig. 2. X-ray diffraction patterns for (a) VAlO 20 800 (unmarked phases correspond to $V_2O_5 \cdot H_2O$; PDF 21-1432) and (b) VAlF 20 800 (unmarked phases correspond to SiO_2; PDF 86-2327).

After calcination at 800 °C, new and well crystallised phases appear for the VO_x doped aluminium oxide as well as for aluminium fluoride catalysts (Fig. 2). The existence of ε-Al_2O_3 beside $V_2O_5 \cdot H_2O$ could be proven in the case of the oxide catalyst (Fig. 2a). Surprisingly, no crystalline fluoride phase was formed during the thermal treatment of the fluoride catalyst. Instead, the formation of κ-Al_2O_3 and small amounts of mullite ($Al_5SiO_{9.5}$) was observed by XRD measurements (Fig. 2b). The silicon impurity may be caused by the reaction between hydrogen fluoride, formed during pyrolysis of VO_xF_y-species and the glass vessel.

3.2. Raman

For the VO_x doped oxyfluorides it was not possible to analyse the vanadium species by Raman spectroscopy at all because of the fluorescent character of the samples.

The Raman spectrum of the vanadium doped oxide is given together with those of V_2O_5 in Fig. 3. In comparison to V_2O_5 the signal-to-noise ratio registered for vanadium doped oxide is worse which points to a low V^V content in the sample. It is well known that VO^{2+} species containing vanadium (IV) are hardly visible in the Raman spectra [22]. The observed Raman bands of vanadium doped oxide are broad and occur at very different wave numbers from those of V_2O_5.

V–O–V bridging vibrations are responsible for Raman bands at 493, 855 and 942 cm^{-1}. The small band at 1048 cm^{-1} is caused by terminal ($V^V = O$) vibrations of VO_x-species. The low wave number of 350 cm^{-1} might origin from Al–O–Al vibrations of the pseudoboehmite sample.

The Raman spectroscopy of the VO_x doped aluminium oxide calcinated at 800 °C confirms the findings of XRD analysis. The formation of V_2O_5 at higher temperatures is proven by the characteristic bands at 997, 708, 286, 196, 147 and 102 cm^{-1}.

3.3. ^{27}Al MAS NMR

The ^{27}Al MAS NMR spectra of both undoped and VO_x doped oxide and fluoride solids along with the calcined samples are shown in Figs. 4 and 5. Fig. 4 includes the complete spectra with all spinning side bands obtained at a spinning speed of 14.8 kHz with the corresponding central transitions given as insets. Whereas the spread of the spinning side bands is very similar comparing the respective undoped and doped samples (cf. Fig. 4a–d), distinct differences exist in the shape of the central transitions.

In the oxides, aluminium has mainly a sixfold oxygen coordination (AlO_6) with the maximum of the central transition at 6.6 ppm. However, in the undoped sample (Fig. 4c) about 2% of the aluminium atoms are in a fourfold oxygen coordination (AlO_4), clearly indicated by the position of the central line at 58 ppm. After VO_x doping the latter contribution is remarkably reduced (Fig. 4d). The main contribution of AlO_6-species to the integral intensity is in agreement with previous findings reported for boehmite and pseudoboehmite samples [23].

Calcination at 800 °C led to pronounced changes in the local coordination of aluminium. Comparing Fig. 5a with c, a clear shift in the integral intensity from sixfold to fourfold Al-coordination can be observed. For the simulation of Fig. 5c no second-order quadrupolar effects were taken into account. Although they cannot be completely excluded, well crystalline reference samples of Al_2O_3 or even AlF_3 do not show such effects (see also [23]). The decomposition of the ^{27}Al spectrum given in Fig 5c is possible with four different Al-species: two AlO_4-species and two AlO_6-species. An integral intensity of 76% can be

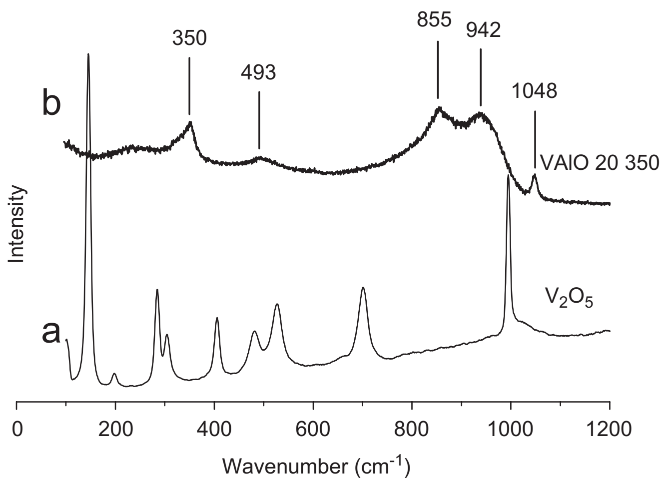

Fig. 3. Raman spectra of (a) V_2O_5 and (b) VAlO 20 350.

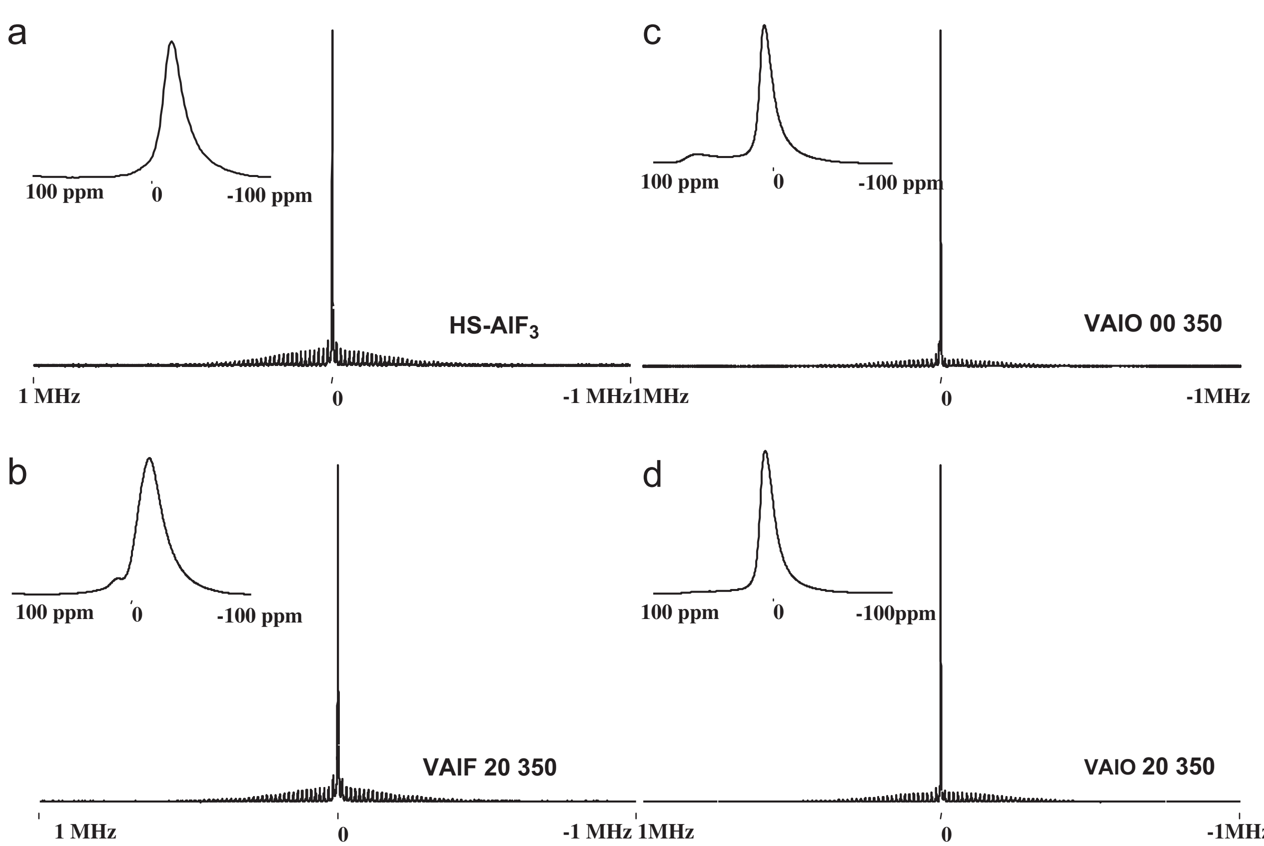

Fig. 4. ^{27}Al MAS NMR spectra taken with the 4 mm probe and a spinning speed of 14.8 kHz of: (a) HS-AlF_3; (b) VAlF 20 350; (c) VAlO 00 350; and (d) VAlO 20 350. The central transitions are given enlarged as insets.

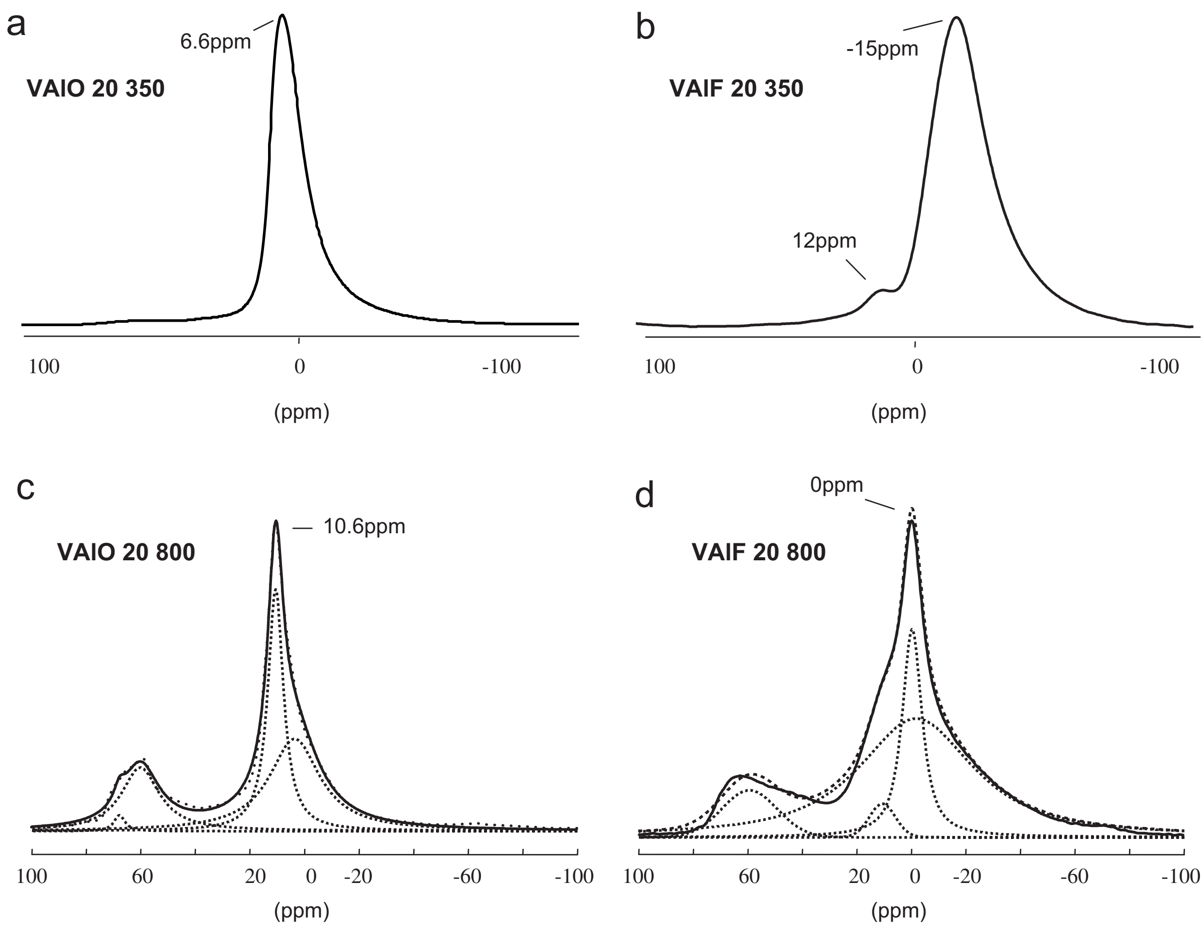

Fig. 5. ^{27}Al MAS NMR spectra (central transitions) taken with the 4 mm probe and a spinning speed of 14.8 kHz of: (a) VAlO 20 350; (b) VAlF 20 350; (c) VAlO 20 800, deconvolution by simulation: (AlO_4)-1: $\delta_i = 67.8$ ppm, linewidth: 4.8 ppm; (AlO_4)-2: $\delta_i = 60.2$ ppm, linewidth: 16.9 ppm; (AlO_6)-1: $\delta_i = 10.6$ ppm, linewidth: 6.9 ppm; (AlO_6)-2: $\delta_i = 3.6$ ppm, linwwidth: 22.5 ppm; Lorentzian line shape for all species; and (d) VAlF 20 800, deconvolution by simulation: (AlO_6): $\delta_i = 10.6$ ppm, linewidth: 12.6 ppm, Gaussian line shape; (AlO_4): $\delta_i = 58.8$ ppm, linewidth: 24.7 ppm, Gaussian line shape; (AlF_xO_y)-1: $\delta_i = -4.7$ ppm, linewidth: 49.6 ppm, 15% Gaussian character; (AlF_xO_y)-2: $\delta_i = -0.2$ ppm, linewidth: 9.0 ppm, 15% Gaussian character; solid lines: experimental spectra.

assigned to AlO_6-species. The parameters of simulation are given in the caption to Fig. 5. The ^{27}Al NMR spectra are consistent with the observation of the ε-Al_2O_3 phase by XRD (see Fig. 2a).

The oxyfluorides are characterised by a dominant AlF_6-coordination of aluminium with the maximum of the central line at $\delta = -15$ ppm (Figs. 4b and 5b). The asymmetric shape in the high-field part of the central transition is due to a broad distribution of bond angles and bond lengths within and between the AlF_6-polyhedrons. In contrast to the undoped sample HS-AlF_3 (Fig. 4a), the vanadium doped AlF_xO_y contains additional AlO_6-species ($\delta_I = +12$ ppm) which obviously remained from not completely fluorinated alkoxide.

Substantial changes occur during the thermal annealing of the V/AlF_xO_y samples (cf. Fig. 5d the central lines are given with the same ppm-scale). The fluorine coordination of aluminium is considerably reduced. Now, about 16% of the integral intensity is due to AlO_6 ($\delta_I = 11$ ppm) and AlO_4 ($\delta_I = 59$ ppm) species (see also [23]). A signal at $\delta_I = 0$ ppm contributes with 23% and a further signal with its maximum at -4.7 ppm contributes with 61% to the whole intensity of the central lines. The latter two can be assigned to different AlF_xO_y units.

Neither for VAlF 20 800 nor for VAlO 20 800, an improvement of the central line resolution of the ^{27}Al MAS NMR spectra could be achieved with an increased spinning speed of 30 kHz (not shown here).

3.4. ^{19}F MAS NMR

The ^{19}F MAS NMR spectra of HS-AlF_3, vanadium doped AlF_xO_y and the calcinated oxyfluoride sample is shown in Fig. 6. As observed for HS-AlF_3 (Fig. 6a), only one broad and unstructured ^{19}F signal is observed for the V/AlF_xO_y (Fig. 6b). An additional broadening in the ^{19}F NMR spectrum of VAlF 20 350 due to V^{4+} can be excluded. For security reasons the spinning speed was not enlarged for the oxyfluoride solid. The strong homonuclear dipolar coupling prevents the observation of further details and leads to such broad lines. The value of the isotropic chemical shift of -161 ppm is slightly down-field shifted

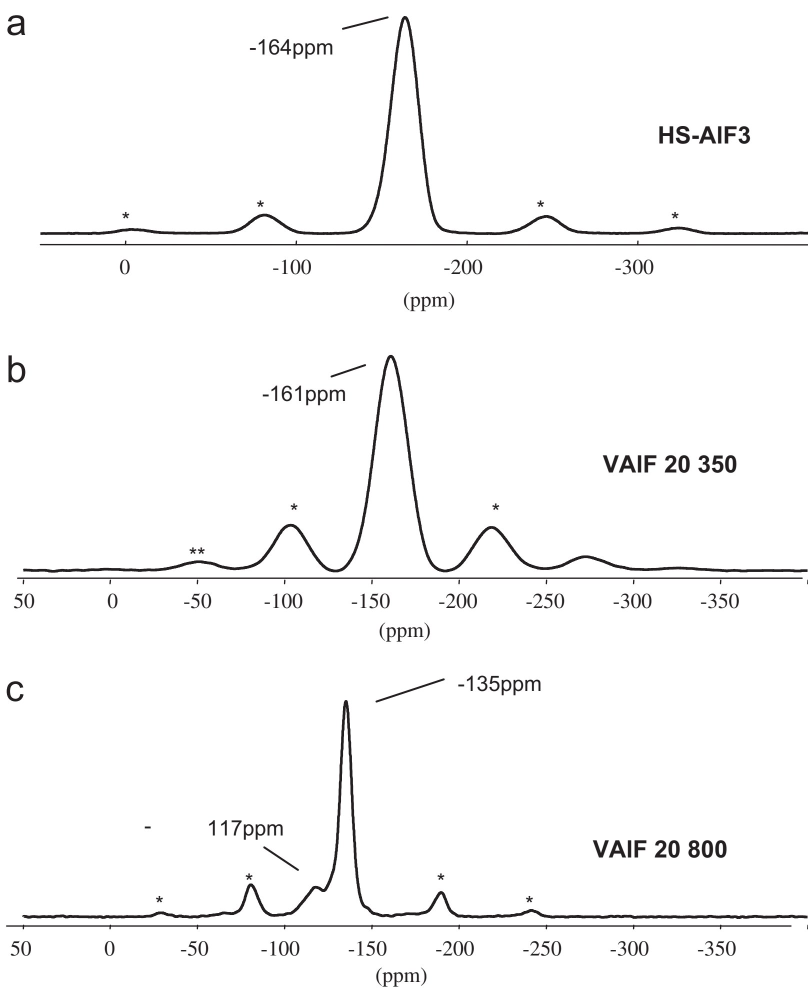

Fig. 6. ^{19}F MAS NMR spectra of (a) HS-AlF_3 ($\nu_{rot} = 30$ kHz), (b) VAlF 20 350 ($\nu_{rot} = 20$ kHz), and (c) VAlF 20 800 ($\nu_{rot} = 20$ kHz), deconvolution by simulation: V_1 (AlF_xO_y): $\delta_{i1} = -135.1$ ppm, linewidth: 6.8 ppm, Intensity: 85%; V_2 (AlF_xO_y): $\delta_{i2} = -117.0$ ppm, linewidth: 12.3 ppm, Intensity: 15% (*: spinning side bands).

with respect to -164 ppm of the ^{19}F signal in HS-AlF_3. Bearing in mind the same ppm-scale in Fig. 6b and c it becomes obvious that a new fluorine environment is formed as a result of the thermal annealing up to 800 °C. Two new and more narrow species with chemical shift values of $\delta_{i1} = -135$ ppm and $\delta_{i2} = -117$ ppm, respectively, can be observed (Fig. 6c). These values are comparable to those obtained by Chupas et al. [24] and were assigned to different AlO_xF_{6-x} species.

The typical ^{19}F signal for fluorine in aluminium fluoride, although disordered, disappeared after annealing.

3.5. ^{51}V MAS NMR

Fig. 7a–d depicts the ^{51}V MAS NMR spectra of the oxyfluoride and oxide solids including all spinning side bands along with the reference materials V_2O_5 and VOF_3. The slightly distorted VO_6 coordination of V^V in V_2O_5 leads to a value of the isotropic chemical shift of -615 ppm (Fig. 7a) as also described in the literature [25,26]. In the VO_x doped oxide a V_2O_5 like NMR signal could not be found which is in agreement with the findings of Raman spectroscopy (Fig. 3). A new signal at -582 ppm, slightly overlapped with spinning side bands, has a value of the isotropic chemical shift which is, according to Ref. [27] in the typical range for distorted corner-shared VO_4 tetrahedrons.

Beside this new signal, a very broad and asymmetric spread of the spinning side bands has been observed. In the high-field part of the spectrum (Fig. 7b) a narrow signal of ^{27}Al is visible in addition, which is due to the large sweep width of 2 MHz chosen for the measurement. Moreover, the spinning side bands of ^{51}V and ^{27}Al seem to overlap. Also, it seems to be possible that the large V^{IV} content of the sample strongly influences the position of the ^{51}V chemical shift and leads to a high-field shift of the V^V signals as also discussed by Delmaire et al. [28].

Calcination of this sample leads to a comprehensive reorganisation of the matrix and phase separation as already found by XRD and ^{27}Al MAS NMR. V^V is not anymore implemented in the matrix so that the typical signal of ^{51}V is similar to that of V^V in V_2O_5

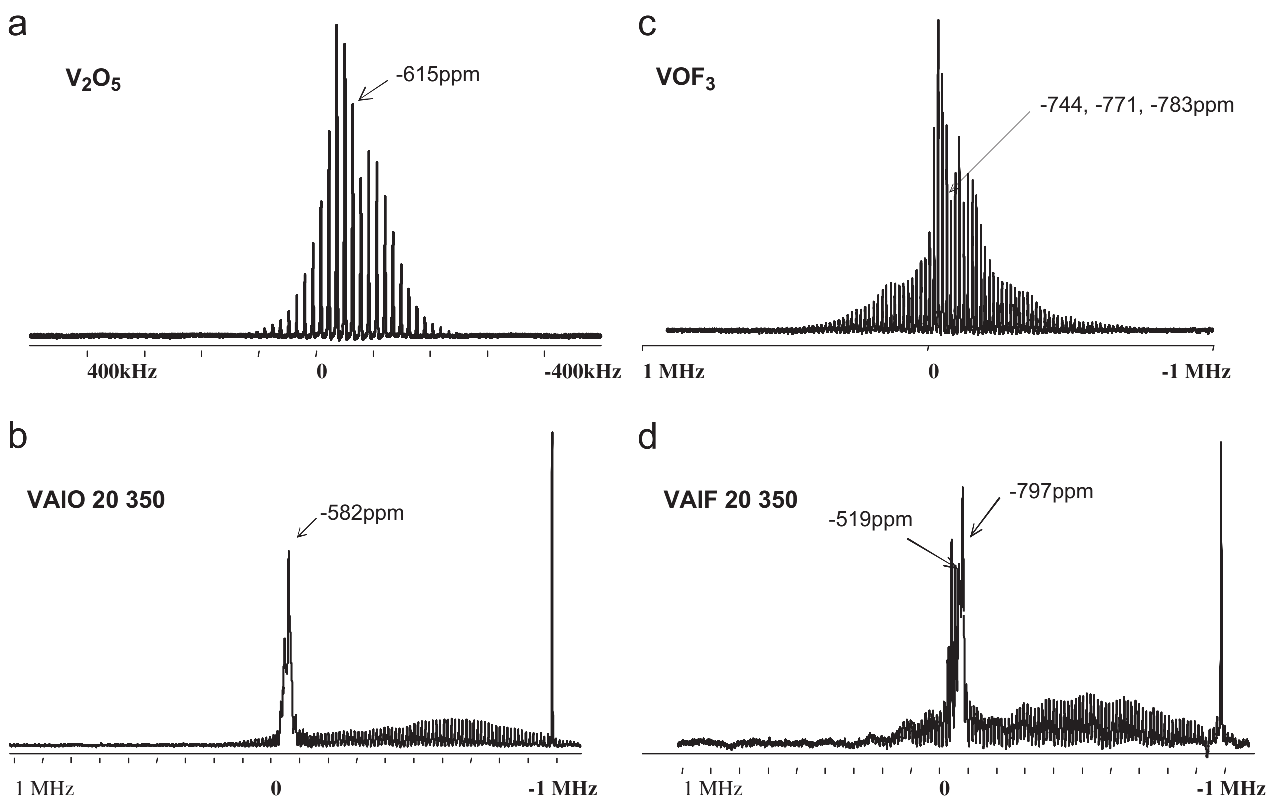

Fig. 7. ^{51}V MAS NMR spectra of (a) V_2O_5 ($\nu_{rot} = 14$ kHz), $\delta_i = -615$ ppm; (b) VAlO 20 350 ($\nu_{rot} = 13$ kHz), $\delta_{i1} = -582$ ppm; (c) VOF_3 ($\nu_{rot} = 15$ kHz), $\delta_{i1} = -744$ ppm, $\delta_{i2} = -771$ ppm, $\delta_{i3} = -783$ ppm, and (d) VAlF 20 350 ($\nu_{rot} = 13$ kHz), $\delta_{i1} = -519$ ppm, $\delta_{i2} = -797$ ppm; the isotropic chemical shifts are indicated in the figure by arrows.

($\delta_I = -611$ ppm; cf. Fig. 8c in comparison to Figs. 8a and 7b). Calcination in air enlarged the V^V content in the matrix with the consequence of a lower number of accumulations necessary to obtain a similar signal-to-noise ratio.

Three ^{51}V species are distinguishable for the VOF_3 sample and can be attributed to three different V positions in the solid (Fig. 7c).[1] Their isotropic values of the chemical shift of $\delta_{I1} = -744$ ppm, $\delta_{I2} = 771$ ppm, and $\delta_{I3} = -783$ ppm are all in the range which can be expected for mostly fluorine coordinated V^V species (see also measurements of solutions [29,30]). The wide spread of spinning side bands of these species can be explained by large anisotropies of the chemical shift and strong quadrupolar interactions. The sweep width of 2 MHz (Fig. 7c) has to be kept in mind in comparison with 1 MHz for V_2O_5 (Fig. 7a).

About 85,000 accumulations have been necessary to record the ^{51}V MAS NMR spectrum of V/AlF_xO_y (cf. Figs. 7d and 8b). A low V^V content and also an unusual chemical shift range due to V^{IV} ions might be the reason for that. In applying different spinning speeds two different V^V-species could be identified with $\delta_{I1} = -519$ ppm and $\delta_{I2} = -797$ ppm. According to the reference substances, the first one should be an oxygen coordinated vanadium species, whereas the second one has at least a partial fluorine coordination, e.g. $[VOF_4]^-$ or VOF_3 (see [30]). Comparing Fig. 7d with b, the general spectral pattern is similar and supports the assumption of the influence of V^{IV} on the line positions as mentioned above.

After calcination the local environment of V^V changes dramatically and as a result two species at $\delta_{I1} = -609$ ppm and $\delta_{I2} = -687$ ppm occur, which were not observed before (Fig. 8d). A comparison with chemical shift values of solution NMR [30] excludes a fluorine coordination at V^V sites now. The spread of the spinning side bands is comparable to those of VAlF 20 350 (Fig. 7d), the V^V content however, is again drastically increased after thermal annealing in air, so that an accumulation number of 2048 was sufficient now (Fig. 8d).

3.6. ESR

The X band ESR spectra of VO_x doped aluminium oxyfluorides and -oxides are depicted along with those obtained after thermal annealing in Fig. 9. The spectra recorded both at room temperature and at 77 K give unambiguous evidence of a large amount of V^{IV} ($3d^1$) species in all samples. In all cases the hyperfine coupling of the unpaired electron of V^{IV} to its nucleus could be resolved indicating an incorporation of V^{IV} as separated point defects into the matrices. However, the lines are not

[1]X-ray structural data of VOF_3 are not available so far.

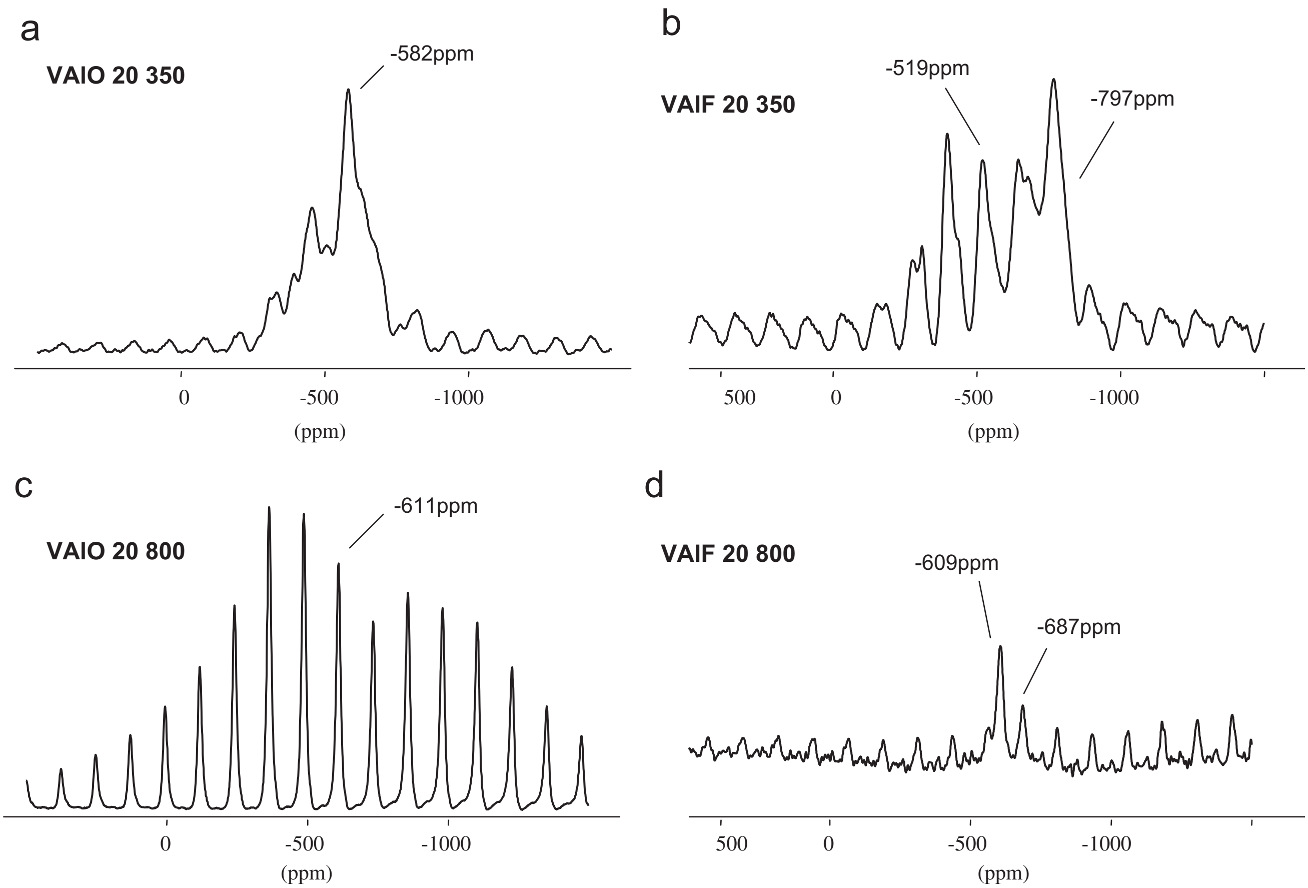

Fig. 8. ^{51}V MAS NMR spectra (central transitions) taken with the 4 mm probe and a spinning speed of $\nu_{rot} = 13$ kHz of: (a) VAlO 20 350, (b) VAlO 20 800, (c) VAlF 20 350, and (d) VAlF 20 800; values and positions of the isotropic chemical shifts are given in the spectra.

as narrow as they can be expected to be for V^{4+} doped well crystalline phases, interactions are present. Furthermore, the unusual shape (see arrows in Fig. 9a) supports the idea of the existence of at least two or more $V^{IV}O_x$ species with an axial symmetric environment in VAlF 20 350. Two different hyperfine coupling constants (hfcc) could be determined as $A_{||1}$~21.8 mT and $A_{||2}$~18.8 mT. A fluorine coordination is suggested for the first species due to the comparably large value of $A_{||1}$. The second species has a hyperfine coupling constant ($A_{||2}$) typical for VO^{2+}-species in oxide matrices [22 and refs. therein].

After annealing at 800 °C, the V^{IV} content is considerably reduced to about 30% of the original V^{IV} content prior to calcination (see Fig. 9b, sample VAlF 20 800) and a new V^{IV} species with a hfcc of $A_{||3}$~16.4 mT, typical for a vanadium–oxygen coordination is formed. The two former species disappear.

The intensities of the ESR spectra of VAlO 20 350 and VAlO 20 800 taken at 77 K are nearly unchanged (see Fig. 9c and d). It means that in contrast to the fluoride catalyst (see Fig. 9a and b) there is nearly no change in the V^{IV} content at calcination. However, changes in the local structure of VO_x species in these samples is manifested by an increase of the hyperfine coupling constant $A_{||}$ from about 16 to 17.7 mT at calcination.

ESR measurements at 4.2 K did not point to the existence of V^{III} species in the samples. However, they gave evidence for the existence of Fe^{III} species in the matrix ($g' = 4.3$, not shown here) possibly introduced with the chemical during the preparation.

4. Discussion

Based on the results above it can be concluded that VO_x doped oxide and oxyfluoride catalysts studied here have several properties in common.

Both are highly disordered solids with a mesoporous structure as previously discussed in [17]. VO_x units can be incorporated in the matrices and are dispersed in the respective solids. In both matrices vanadium coexists in two oxidation states as V^{IV} and V^{V}, with V^{IV} as the dominating species in vanadium doped AlF_xO_y. The calcination in air at higher temperature (800 °C) leads to a comprehensive reorganisation of the matrices. Most of the V^{IV} is oxidised to V^{V}. Although the incorporation of VO_x in the fluoride and oxide bulks is quite different, their local structure is very similar after calcination. In addition, all spectroscopic data indicate the formation of transition aluminas (ε- and κ-Al_2O_3) as very similar supports for VO_x at 800 °C.

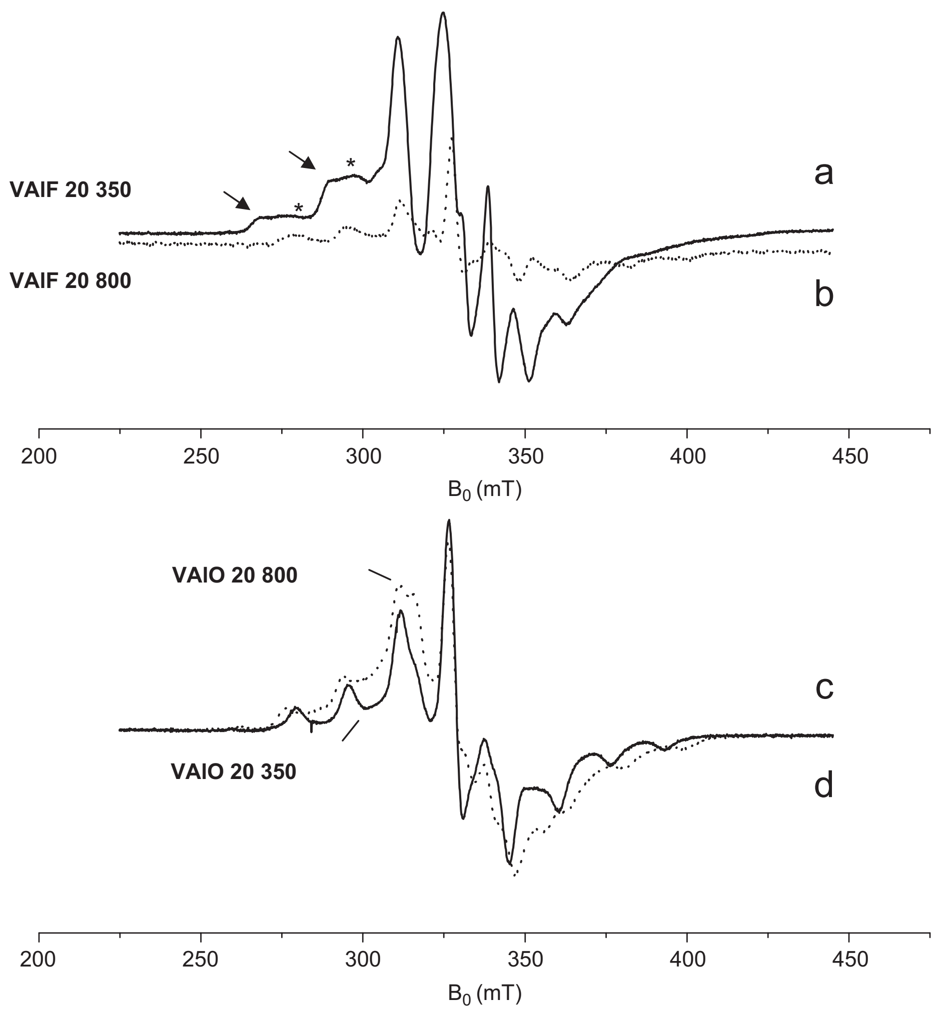

Fig. 9. X-band ESR spectra (77 K) of: (a) VAlF 20 350, $A_{||1}$~21.8 mT (→), $A_{||2}$~18.8 mT (*), (b) VAlF 20 800 (enlarged by a factor of 1.56), (c) VAlO 20 350, and (d) VAlO 20 800.

Despite these common features several peculiarities exist, which can be directly related to their specific chemical nature as fluoride or oxide system.

In the oxide system the VO_x doping decreases the number of observable AlO_4 sites whereas the AlO_6 sites remain unchanged. It means that doping occurs obviously on AlO_4 sites with the formation of V^VO_4 bridging units ($\delta_{I(51V)} = -582$ ppm). Also Raman data, allowing the observation of such –V–O–V– bridging vibrations, support therewith the MAS NMR results. The reason, why vanadium preferably replaces tetrahedrally coordinated aluminium is still unclear. Possibly, the AlO_4 units are easier accessible for the vanadium species due to the porous structure of the solids.

Calcination at 800 °C oxidises present $V^{IV}O_x$ species to V^VO_z, removes VO_4 units from the fourfold Al positions and finally leads to a phase separation into $V_2O_5 \cdot H_2O$ and ε-Al_2O_3. The latter possesses AlO_6 as well as AlO_4 coordination polyhedrons.

For the oxyfluoride system V/AlF_xO_y the only structural information comes from magnetic resonance data. The number of V^V ions incorporated in the bulk is extremely low and occurs as VO_6 and partially fluorinated VO_xF_y species. Rests of AlO_6 polyhedrons indicate that not all of the Al-O*i*Pr groups are consumed as anchor groups for functionalisation with VO_x.

Surprisingly, calcination in air reduces the fluorine content of the matrix considerably with the result that no separate aluminium fluoride phase exists. Only few AlO_xF_y species (see also [24]) can be detected now whereas V–F species disappeared. Beside a reduction of the number of V^{IV} species, even here a transition alumina (κ-Al_2O_3) with AlO_4 and AlO_6 polyhedrons is formed. New VO_x species are formed which were not present before. The loss of fluorine can be explained by the formation of volatile VO_xF_y compounds or fluorine containing vapour phase complexes well known for the AlF_3 system [31].

5. Conclusion

Using a modified sol–gel technique for preparing vanadium doped aluminium oxides and oxyfluorides, highly distorted solids with well-dispersed VO_x species are obtained. For a thorough structural investigation of the mainly amorphous samples, MAS NMR spectroscopy in combination with ESR has to be applied. It can unambiguously derived from the spectroscopic results that vanadium exists in two oxidation states (V^{IV} und V^{V}) after thermal treatment at 350 °C. In the oxyfluoride system both, aluminium and vanadium are coordinated by oxygen as well as by fluorine. After calcination at 350 °C no suggestion for the formation of V_2O_5 was obtained from different spectroscopic measurements, although the interpretation of the ^{51}V MAS NMR-spectra was difficult due to the high V^{IV} content of the solids.

The calcination in air at 800 °C, however, leads to a comprehensive reorganisation of the coordination. Especially the fluorine coordination of aluminium and vanadium decreases considerably during annealing. Simultaneously, the V^{IV} content is dramatically reduced resulting from the oxidation to V^{V}. With the vanadium doped aluminium oxides, the structural reorganisation is accompanied by a phase separation into ε-Al_2O_3 and $V_2O_5 \cdot H_2O$.

Acknowledgments

This work was supported by 6th Framework Program (FUNFLUOS, Contract No. NMP3-CT-2004-5005575). The authors thank Dr. D. Heidemann for performing some MAS NMR, Dr. A. Zehl and Prof. Dr. R. Stoesser for ESR and Dr. K. W. Brzezinka for Raman measurements.

References

[1] E.A. Mamedov, V. Cortes Corberan, Appl. Catal. A 127 (1995) 1.
[2] B.M. Weckhuysen, D.E. Keller, Catal. Today 78 (2003) 25.
[3] M.M. Bettahar, G. Costentin, L. Savary, L. Lavalley, Appl. Catal. A 145 (1996) 1.
[4] J.M. Tatibouet, Appl. Catal. A 148 (1997) 213.
[5] J. Keranen, C. Guimon, E. Iiskola, A. Auroux, L. Niinisto, J. Phys. Chem. B 107 (2003) 10773.
[6] O.V. Bujevskaja, A. Brückner, E.V. Kondratenko, D. Wolf, M. Baerns, Catal. Today 67 (2001) 369.
[7] A. Khodakov, B. Olthof, A.T. Bell, E. Iglesia, J. Catal. 181 (1999) 75.
[8] F. Cavani, F. Trifiro, Catal. Today 24 (1995) 307.
[9] A. Adamski, Z. Sojka, K. Dyrek, M. Che, Solid State Ionics 117 (1999) 113.
[10] F. Arena, F. Frusteri, A. Parmalania, Catal. Lett. 60 (1999) 59.
[11] G. Marta, F. Arena, S. Clouccia, F. Frusteri, A. Parmaliana, Catal. Today 63 (2000) 197.
[12] K. Scheurell, E. Hoppe, K.W. Brzezinka, E. Kemnitz, J. Mater. Chem. 14 (2004) 2560.
[13] K. Routray, K.R.S.K. Reddy, G. Deo, Appl. Catal. A 265 (2004) 103.
[14] S.M. Al-Zahrani, B.Y. Jibril, A.E. Abasaeed, Ind. Eng. Chem. Res. 64 (2000) 1729.
[15] A. Hess, E. Kemnitz, J. Catal. 149 (1994) 449.
[16] E. Kemnitz, U. Gross, S. Ruediger, C.S. Shekar, Angew. Chem. Int. Ed. 42 (2003) 4251.
[17] K. Scheurell, E. Kemnitz, J. Mater. Chem. 15 (2005) 4845.
[18] Powder Diffraction File, ICPDS-ICDD2001.
[19] D.G. Cory, W.M. Ritchey, J. Magnet. Res. 80 (1988) 128.
[20] D. Massiot, F. Fayon, M. Capron, I. King, S. Le Calvé, B. Alonso, J.O. Durand, B. Bujoli, Z. Gan, G. Hoatson, Magn. Reson. Chem. 40 (2002) 70.
[21] M. Nofz, R. Stößer, G. Scholz, I. Dörfel, D. Schultze, J. Europ. Ceram. Soc. 25 (2005) 1095.
[22] A. Brückner, M. Schneider, D. Herein, G. Scholz, D. Heidemann, U. Bentrup, M. Kant, J. Catal. (2007), in press, doi:10.1016/j.jcat.2006.11.004.
[23] R. Stösser, G. Scholz, J.Y. Buzaré, G. Silly, M. Nofz, D. Schultze, J. Am. Ceram. Soc. 88 (10) (2005) 2913.
[24] P.J. Chupas, D.R. Corbin, V.N.M. Rao, J.C. Hanson, C.P. Grey, J. Phys. Chem. 107 (2003) 8327.
[25] A.A. Shubin, O.B. Lapina, D. Courcot, Catal. Today 56 (2000) 379.
[26] B.A. Gee, A. Wong, J. Phys. Chem. B 107 (2003) 8382.
[27] O.B. Lapina, A.A. Shubin, D.F. Khabibulin, V.V. Terskikh, P.R. Bodart, J.-P. Amoureux, Catal. Today 78 (2003) 91.
[28] F. Delmaire, M. Rigole, E.A. Zhilinskaya, A. Aboukais, R. Hubaut, G. Mairesse, Phys. Chem. Chem. Phys. 2 (2000) 4477.
[29] R.J. Gillespie, U.R.K. Rao, J. Chem. Soc. Chem. Comm. (1983) 422.
[30] R.C. Hibbert, J. Chem. Soc. Dalton Trans. (1986) 751.
[31] G. Scholz, R. Stösser, J. Fluorine Chem. 86 (1997) 131.